Identification of Large Fullerenes Formed during the Growth of Single-Walled Carbon Nanotubes in the HiPco Process

Sivarajan Ramesh,[†] Bruce Brinson,[‡] M. Pontier Johnson,[‡] Zhenning Gu,[†] Rajesh K. Saini,[†] Peter Willis,[†] Terry Marriott,[†] W. E. Billups,[†] J. L. Margrave,[†] Robert H. Hauge,[†] and Richard E. Smalley*[,†]

Carbon Nanotechnology Laboratory, Center for Nanoscale Science and Technology, Department of Chemistry, Department of Electrical and Computer Engineering, MS-100, Rice University, 6100 Main Street, Houston, Texas 77005

Received: September 20, 2002

Iron-catalyzed, gas-phase disproportionation of carbon monoxide under high pressures is known to produce single-walled carbon nanotubes (SWNT) in high yields. Small amounts of nontubular nanocarbons and iron encapsulated-graphitic shelled nanoparticles are produced concomitantly. Differences in the oxidation kinetics among the SWNT, nontubular carbon, and iron core−graphitic shell nanoparticles have been exploited as a tool for the quantitative determination of high-molecular-weight nontubular, carbon products. The nontubular carbon materials were eliminated by selective oxidation wherein the raw material was subjected to increasing oxidation thresholds followed by acid leaching in an aqueous or gas−solid reaction. Relative concentrations of nontubular nanocarbons in differentially oxidized samples were determined employing laser desorption ionization-mass spectrometry (LDI-MS) with C_{60} and bismuth triphenyl as internal markers. The identity of the nontubular carbon was examined by nondestructive extraction through fluorination in a gas−solid reaction followed by LDI-MS and electron microscopic and polarized Raman spectroscopies. The extracted nontubular carbon was found to be comprised predominantly of large, closed-shell carbon structures spanning the range of C_{120} to C_{400}.

Introduction

Catalyzed gas-phase pyrolysis of carbon source gases in a continuous flow process has recently emerged as a promising alternative to conventional arc growth and laser growth methods for the synthesis of carbon nanotubes.[1] Smaller hydrocarbons such as C_2H_4 and CH_4 when used as feedstock in catalytic pyrolysis processes do yield single-walled carbon nanotubes.[2,3] However, a major disadvantage with smaller hydrocarbons as feedstock is their lower pyrolysis temperature (<800 °C) resulting in the formation of larger quantities of graphitic carbon. This serious limitation was overcome by Smalley and coworkers by employing carbon monoxide as the carbon source feedstock in an iron-catalyzed high-pressure disproportionation reaction known as the HiPco process.[4,5] In this process, carbon monoxide is disproportionated into elemental carbon and carbon dioxide (Boudard reaction) at a temperature of ∼1000 °C at pressures ranging from 10 to 100 atm.

Although the experimental parameters influencing the HiPco process have been optimized for maximum yields of SWNT, the inherent mechanism of the catalyzed growth process results in the concomitant formation of approximately 10% of nontubular carbon products. In addition, the termination of tube growth is accompanied by the growth of graphitic carbon layers as the iron particles increase in size, leading to the formation of iron core−graphitic shell nanoparticles in the diameter range of 1−5 nm. Accordingly, separation of pure SWNT with minimum chemical modification from a mixture of nontubular carbon and iron−carbon nanoparticles has been extensively studied resulting in specific purification protocols.[6−8] Invariably, such protocols are based on exploiting the well-known differences in oxidation thresholds for different forms of carbons. For example, the fullerenic molecules and SWNT are known to be oxidized at significantly lower temperatures than graphitic carbons under identical ambient oxidizing atmosphere.[9] Graphitic carbon coated in the form of a thin layer on iron nanoparticles is catalytically oxidized at lower temperature. Due to the complexity of the reaction product mixture and the resultant differences in oxidation chemistry used to separate them, the nature of the nontubular carbon products and the mechanistic aspects of their oxidative elimination has remained elusive. Hence, understanding the identity and formation mechanism of the high-molecular-weight nontubular nanocarbon products is important for the optimization of yield and quality of the single-walled carbon nanotubes.

In this study, we have focused on the chemical identity of the high-molecular-weight nontubular carbons formed in the HiPco process employing thermogravimetric analysis (TGA), high-resolution transmission electron microscopy (HRTEM), and laser desorption ionization-mass spectrometry (LDI-MS) as analytical tools. An analytical technique employing a combination of C_{60} and bismuth triphenyl as concurrent internal standards to quantify the relative concentrations of nontubular carbons has been developed and employed. Further, the nontubular nanocarbon materials were separated nondestructively by a fluorination procedure followed by extraction in tetrahydrofuran. HRTEM, LDI-MS, and Raman spectroscopic investigations of the extracted nontubular carbon provided additional clues to establish the identity of the nontubular carbon products. The

* Corresponding author.
[†] Department of Chemistry.
[‡] Department of Electrical and Computer Engineering.

10.1021/jp027043h CCC: $25.00 © 2003 American Chemical Society
Published on Web 01/21/2003

nontubular carbon was found to be nonvolatile even at temperatures as high as 800 °C and was found to be composed of large closed-shell carbon structures falling in the class of giant fullerenes.[10,11]

Experimental Section

Single-Wall Carbon Nanotube Raw Soot Production. The raw carbon product, **1**, consisting mainly of SWNT, nontubular carbon, and iron-graphitic nanoparticles, was synthesized by high-pressure disproportionation of carbon monoxide at 30 atm and conditions described in detail elsewhere.[4,5]

Argon Annealed SWNT Raw Product. The volatile carbon content in the sample was determined by heating the raw carbon product, **1**, in a tubular quartz oven at 800 °C for 3 h under flowing argon to produce **2a**.

Oxidative Elimination Reactions. The raw carbon, **1**, was subjected to varying degrees of oxidation to eliminate the nontubular carbon. Oxidative soft baking was accomplished by placing ~5 g of accurately weighed raw carbon soot in a glass beaker, at 250 °C in an ambient oven. Water vapor-saturated air was supplied by a continuous flow of air bubbled through a water column maintained at 60 °C. The samples were heated for 5 h, 10 h and 20 h (**3a**, **4a**, and **5a**, respectively).

Acid Digestion of Catalytic Fe/Fe−Graphite Nanoparticles. *1. Concentrated HCl.* Catalyst iron/iron oxide particles in the differentially oxidized samples were removed by placing the samples in excess concentrated HCl for 12 h. The acid-digested **3b**, **4b**, and **5b** were washed repeatedly with deionized water and centrifuged until the supernatant liquid was free of color and neutral to litmus paper.

2. HCl (gaseous)/Argon Annealing. In a second set of experiments, iron in the soft baked samples was removed in a gas−solid reaction by leaching the iron/iron oxide impurities with gaseous HCl. Samples of **3a**, **4a**, and **5a**, 100 mg, were heated in a quartz tubular reactor tube for 1 h at 800 °C under a flowing stream of hydrogen chloride gas (70 cm^3/min 10% HCl + 50 cm^3/min argon). The purification yielded **3c**, **4c**, and **5c**.

Fluorination of Raw SWNTs. In a separate gas−solid reaction, the raw, Ar annealed carbon, **2a**, was fluorinated for 12 h at 150 °C in a specially designed stainless steel reactor.[12] A gaseous fluorinating mixture of helium, fluorine, and hydrogen (40:6:2) with a total flow rate of 48 cm^3/min was used for the fluorination to yield **2b**.

Extraction with THF. Fluorinated **2b** was dispersed in dry tetrahydrofuran by mild sonication in a sonication bath at room temperature. The sample was filtered through a 0.2 μ PTFE filtation membrane. The filtrate containing the THF extract, **2c**, comprised of solubilized carbon was analyzed by HRTEM and LDI -MS.

Characterization. The samples wherever applicable, were analyzed for their total carbon content by thermogravimetry in air (flow rate 100 cm^3/min; heating rate 5 °C/min) employing a TA-SDT-2960 DTA-TGA analyzer. The samples were examined for their content and morphology by transmission electron microscopy (TEM) employing a JEOL 2010 HRTEM operated at 100 kV (spot size 2, $\alpha = 1$). Copper grids, 200 mm, with a lacey carbon support film were used for sample preparation. The soft baked samples (**3a**, **4a**, and **5a**) were examined by laser desorption ionization-mass spectrometry (LDI-MS) employing a Bruker, Biflex-III LDI-MS spectrometer described elsewhere.[13] A nitrogen laser operating at 337 nm was used for desorbing the carbon samples. Relative concentrations of desorbable carbon species in the differentially oxidized samples were determined by employing C_{60} and bismuth triphenyl as internal standards. Typically the samples were prepared by suspending 10 mg of the sample in 1 mL of 1% solution of C_{60} in chlorobenzene and sonicating for 30 min in a bath sonicator. On completion of sonication, 1 mL of a 1% solution of bismuth triphenyl in chlorobenzene was added and shaken well. (Note: Sonication of a suspension of bismuth triphenyl may result in the formation of bismuth colloid.) A drop of the suspension was placed on a stainless steel substrate plate in the LDI-MS analyzer and dried. Raman spectra where applicable were recorded on solid samples employing a Renishaw polarized laser Raman spectrometer with a diode laser emitting 780 nm as the excitation source.

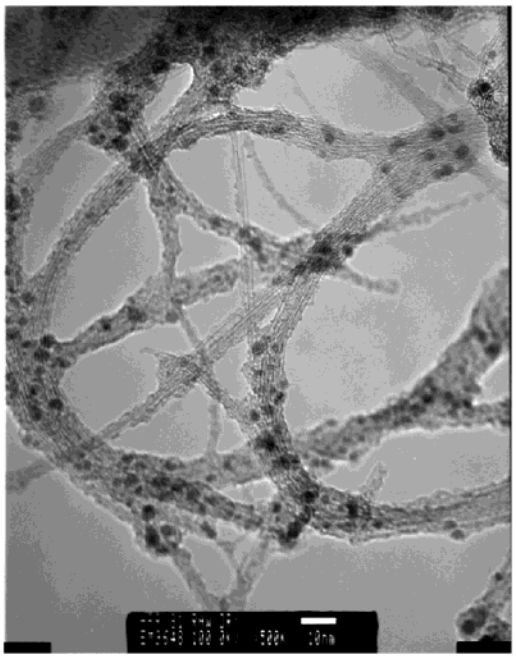

Figure 1. Transmission electron photomicrograph of raw HiPco soot. The sample consists predominantly of bundles of single-walled carbon nanotubes. Iron core −graphitic shell nanoparticles of approximate diameter 3 nm are seen as dark spots. The nontubular nanocarbon formed concomitantly forms a coating on the SWNT bundles. The scale bar is 10 nm.

Results and Discussion

A high magnification transmission electron photomicrograph of **1** is shown in Figure 1. The sample consists predominantly of SWNT, small portions of iron−graphitic core−shell nanoparticles (dark particles), and nontubular carbonaceous species mainly as a coating on the tubular carbon. The TGA weight loss patterns in air for raw product sample **1**, soft baked samples **3a**, **4a**, and **5a**, and argon annealed sample **2a** are shown in Figure 2 The raw product **1** registered an ash content of 29.5%, primarily Fe_2O_3. A notable feature in the case of **1** was an increase in sample weight (~10%) in the temperature range 200−280 °C. This is attributed to the oxidation/hydroxylation of carbon and to a larger extent from the oxidation of iron in the iron-graphitic core shell nanoparticles.

Complete oxidation of iron nanoparticles in all of soft baked **3a**, **4a**, and **5a** was evidenced by the lack of weight gain in this temperature range. **3a**, soft baked only for 5 h, registered an ash content of 23.4%, a value smaller than those for the starting raw material **1**. This observation, which otherwise appears to indicate an increase in the C/Fe mole ratio in an oxidized sample can be understood from the relative kinetics of two competing

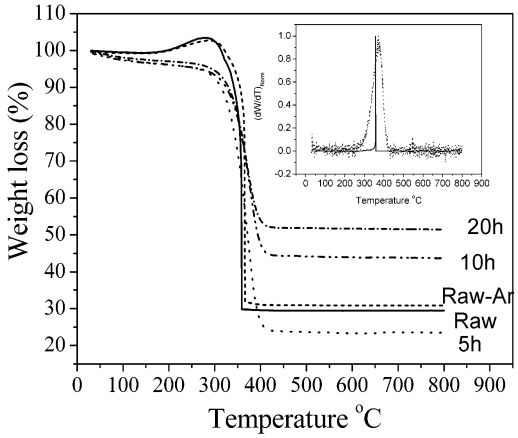

Figure 2. The TGA weight loss patterns in air for raw HiPco soot (**1**), samples soft baked for varying times (**3a**, **4a**, and **5a**) and argon annealed sample (**2a).** Inset shows the first derivative of the weight loss pattern for the raw Raw HiPco soot (solid line) shows sharp transition indicating the rapid and simultaneous combustion of all types of carbonaceous species present in the system. The dotted curve in the inset is the derivative plot for the sample soft baked for 5 h.

processes that take place during the oxidative hydrolysis of the raw material. In the initial stages, the graphitic carbon is oxidatively hydrolyzed to −OH and −COOH groups with an associated increase in weight. The iron oxide formed during the oxidation of the metallic iron core, in turn catalyzes the combustion of carbonaceous species leading to weight losses.

Consequently, increasing the oxidation times as in the case of samples heated for 10 h and 20 h resulted in increased loss of carbonaceous material as evidenced from an ash content of 43.6 and 51.4% respectively. Notably, **2a**, annealed under argon at 800 °C, registered an ash content of 30.83, very close to that of the raw sample itself. This observation implies the absence of any carbonaceous species that is volatile at least up to 800 °C. Apart from this, **2a** followed the same weight gain pattern as the raw sample in the temperature range of 200−280 °C, verifying the importance of an oxidizing ambient in opening the carbon-shelled iron nanoparticles. Had the core−shell nanoparticles been cracked thermally during the inert gas annealing, the maximum weight gain and the on-set temperature for weight loss would have both been shifted to significantly lower temperatures.

The first derivative of the weight loss pattern (shown as a solid line in the inset of Figure 2) for the raw sample exhibited a very sharp transition indicating the rapid and simultaneous combustion of all types of carbonaceous species present in the system. The maximal rate of weight loss was observed at 330 °C. On the other hand, all the soft baked **3a**, **4a**, and **5a** showed a broadened derivative curve indicating a slowed rate of combustion. The curves were identical for all the soft baked samples (**3a** shown as an example in the inset of Figure 2). The combustion was a single-step process as in the case of the raw **1**. The decreased rate of combustion in the soft baked samples is attributed to the possible presence of hydroxyls and carboxylic acid groups. However, the combustion catalyzed by iron/iron oxide was still rapid enough such that the presence of carbanoceous species of different oxidation thresholds cannot be differentiated in the derivative plots.

The weight loss patterns in the case of samples leached with hydrochloric acid in solution phase (**3b**, **4b**, and **5b**) are shown in Figure 3. The difference in ash content in the leached samples was very small, indicating the oxidative cracking of the iron core−graphitic shell nanoparticles has been completed by soft

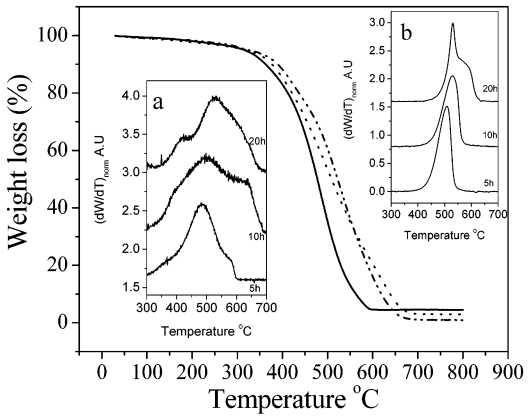

Figure 3. The TGA weight loss patterns for wet acid leached samples that were soft baked for varying times: 5 h (solid line), 10 h (dotted), and 20 h (dot-line-dot). The derivative plots for the TGA weight loss traces are give in inset a. Inset b shows the derivative plots for the corresponding samples leached from iron with gaseous HCl.

baking for durations as low as 5 h. The derivative plots of the same curves are shown in Figure 3, inset a. The derivative plots showed three distinct regions of weight loss. A general feature was the temperature for maximal rate of weight loss shifted to higher temperatures as compared to the non oxidized sample. The differences in the oxidation threshold of the carbon species were less pronounced in the case of samples leached of iron in the gas phase. The derivative plots of the weight loss patterns in the case of gas-phase leached samples are shown in the Figure 3, inset b, for comparison.

The TEM photomicrographs of sample **5a** (soft baked for 20 h) and the corresponding acid-leached **5b** are shown in Figures 4a and 4b, respectively. The soft baked samples consist of SWNT and the iron oxide nanoparticles dispersed throughout the sample. The nontubular carbonaceous species that were present in the raw sample were clearly absent in the soft baked sample, verifying their oxidative elimination. The acid-leached sample consisted of bundles of SWNT and very few iron nanoparticles that were still not exposed to acid leaching. It should be noted that the acid-leached (solution phase, 20 h soft bake) sample still consisted of ∼0.1 at. % of iron impurities as determined from TGA which could account for the smaller weight loss arising from the catalyzed combustion of SWNT at temperatures lower than 450 °C. The preferential oxidation of defective, open-ended, and smaller tubes compared to closed and or larger diameter tubes is well recognized [14] and could account for differences in the oxidation thresholds at higher temperature.

Figure 5 shows the LDI-TOF mass spectra recorded under identical conditions for **1**, **3a**, **4a**, and **5a**, respectively. The raw sample and the samples were soft baked at various soft baking conditions. These are the normalized intensities within each spectra of the samples examined without an internal marker. The raw sample showed a mass spectral span of 1800−4500 u with the maximal intensity at 2600 u. The masses were evenly separated at a spacing of 24 amu, a well-known feature in the mass spectral pattern of fullerenes arising from the loss of C_2 species.[15,16] The integrated intensity of mass spectral lines decreased with increasing oxidation times as can be seen in Figure 5. The mass peak for maximal intensity shifted to 3200 u in the case of the sample soft baked for 5 h. Although this established that the nontubular carbonaceous species is the origin of the fullerenic C_2 signature in the LDI-MS experiments, two important hurdles were faced in further interpretation of the observed mass spectra. Qualitatively, it was important to

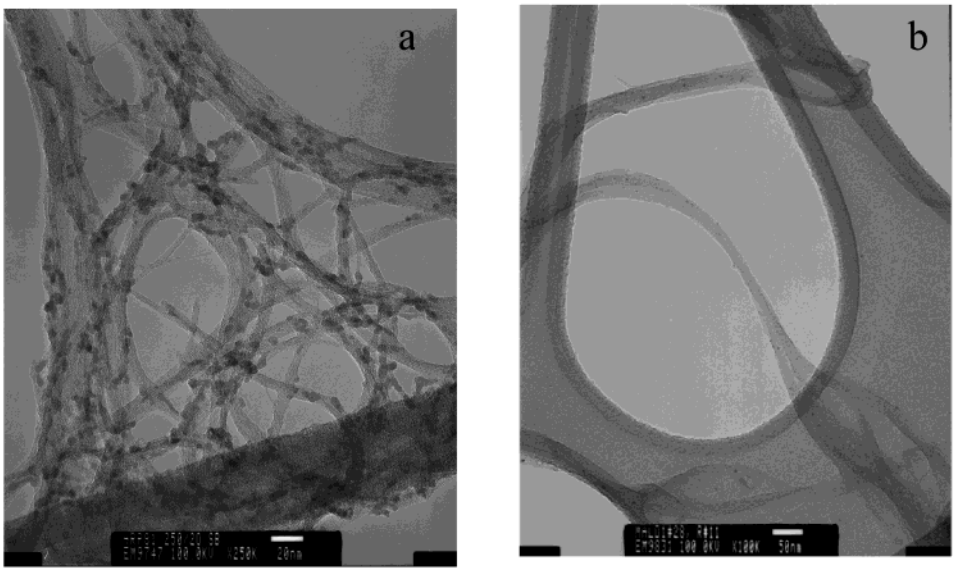

Figure 4. Transmission electron photomicrographs of (a) raw HiPco soot soft baked for 20 h. (**5a**) and (b) the same sample on wet acid leaching. While the oxidized iron nanoparticles are still seen as dark spots in (a), the nontubular carbon observed in the raw soot (see Figure 1) is not seen. The iron oxide nanoparticles are absent in the wet acid leached samples to a large extend.

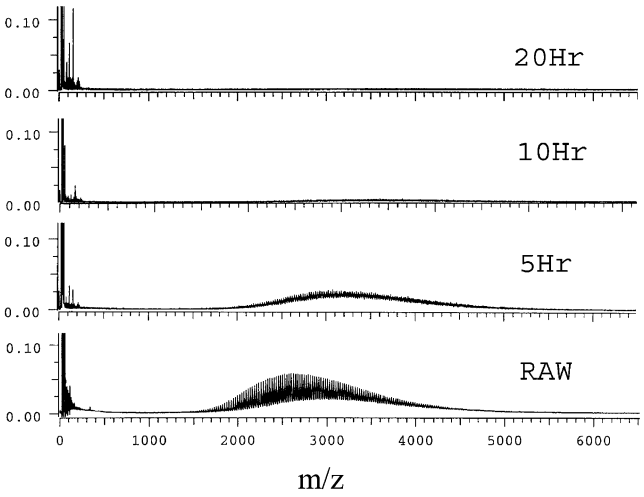

Figure 5. LDI-TOF mass spectral patterns recorded under identical conditions on HiPco raw samples soft baked for varying times. These are the normalized intensities within each spectra on samples examined without an internal marker. The raw sample showed a mass spectral span of 1800−4500 u with the maximal intensity at 2600 u. The masses were evenly separated at a spacing of 24 amu. Note that the mass number for maximal intensity has shifted to higher mass numbers in the oxidized samples indicating lower threshold for low-molecular-weight carbonaceous species. *y*-axis is intensity in arbitrary units.

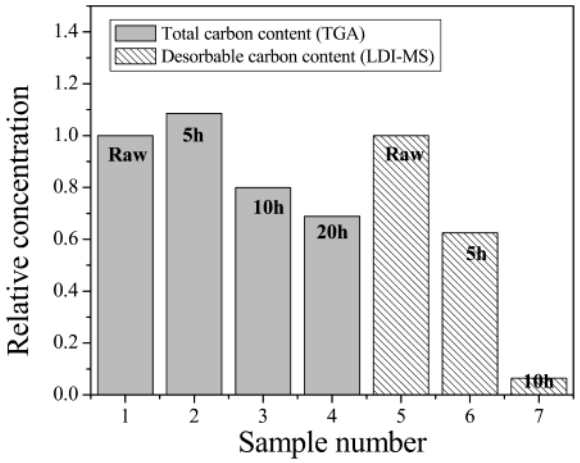

Figure 6. Relative concentrations of total carbon and laser desorbable carbon content. The total carbon contents were determined by thermogravimetry. An apparent slight increase in carbon content in **2** arises from relative weight gain during the oxidation of the raw soot. The desorbable carbon concentration shown in the figure are from experiments marked with C_{60} and bismuth triphenyl. The raw HiPco soot when soft baked for 20 h loses all desorbable carbon.

establish the chemical identity of the nontubular carbon present as such in the HiPco raw material against the possible formation of closed shell carbon clusters during the course of the laser desorption ionization process as part of the LDI-MS experiment. Fullerenes, after all, are formed by laser vaporization of graphitic carbon under conditions that are not very different from those that prevail in the LDI-MS experiment.[17−19] The second problem was about the direct correlating of the observed integrated intensities to relatively quantify the laser desorbable carbon species. The latter problem can be readily overcome by the simple addition of a known quantity of C_{60}, having ionization cross section comparable to the fullerenic carbon, to the test samples as an internal standard. However, the presence of exposed iron oxide nanoparticles was found to affect the desorption of C_{60} from the sample. Under these circumstances, bismuth triphenyl was chosen as a secondary marker because of its lower decomposition temperatures, higher mass, and abundance of bismuth ion. The spectra with internal standards were normalized to have the bimuth mass ion at unit intensity and the ratio of the C_{60}/Bi was taken as a measure to quantify the relative concentrations of desorbable carbon species in the various soft baked samples.

The bar graph in Figure 6 shows the relative concentrations of total and desorbable carbon, respectively, in the case of the soft baked samples. The loss of carbon in the thermal oxidation process includes loss due to the fullerenic species, graphitic shell carbon, and a significant amount of small diameter SWNT. The bar graphs shown in dark gray depict the relative concentration of desorbable carbon determined by LDI-MS. As one would expect, the relative concentration of desorbable carbon decreased rapidly with increasing oxidation times compared to the total carbon content. The nontubular/ desorbable carbon in the sample soft baked for 20 h was found to be practically absent.

If the possible formation of fullerenes in the LDI-MS instrument is to be excluded, then it requires that the nontubular

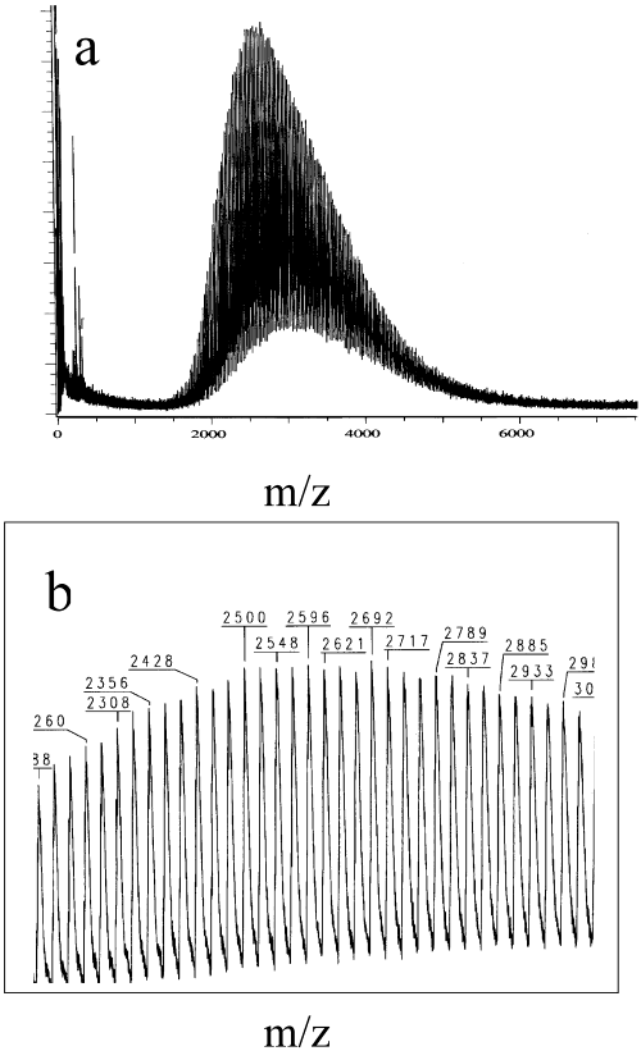

Figure 7. (a) LDI-TOF mass spectra of the sample obtained by extracting the fluorinated raw HiPco soot in tetrahydrofuran. Typically a drop of the THF extract is placed on the stainless steel sample plate and dried before laser irradiation. (b) The magnified view of the central portion of the spectra. The spacing of 24 u arising from the loss of a C_2 species can be seen. *y*-axis is intensity in arbitrary units.

carbon species be non destructively separated from the raw material and its identity verified. The fullerenic carbon in the raw sample was extracted in THF solvent by fluorinating the raw samples as described in the Experimental Section. The nontubular carbon extract in THF, reddish brown in color prepared as described in the Experimental Section, was examined by LDI-MS and TEM. The LDI-TOF mass spectra of flurorinated extract is shown in Figure 7a. The mass spectral pattern matched that of the mass spectral pattern from the raw sample with a maximal intensity at 2600 u. A section of the central portion of this spectrum in an expanded scale is shown in Figure 7b. The mass spectral lines are evenly spaced at 24 u. This feature is a possible outcome of the photofragmentation and contraction of closed shell carbon structures by the successive elimination of a carbon dimers (C_2) or represents the actual size distribution of fullerene species.

The identity of the nontubular species was further examined by transmission electron microscopy of the fluorinated extract. A drop of the extract reddish brown in color was, placed directly on a TEM grid, dried and examined. The TEM micrograph of the nontubular carbon extract recorded at a magnification of 500 000 is shown in Figure 8. The sample was found to contain

Figure 8. Transmission electron micrograph of the sample obtained by extracting the fluorinated raw HiPco soot in tetrahydrofuran. Similar to the LDI-TOF experiments a drop of the THF extract is placed on a holey carbon TEM grid and dried before imaging. Scale bar is 10 nm.

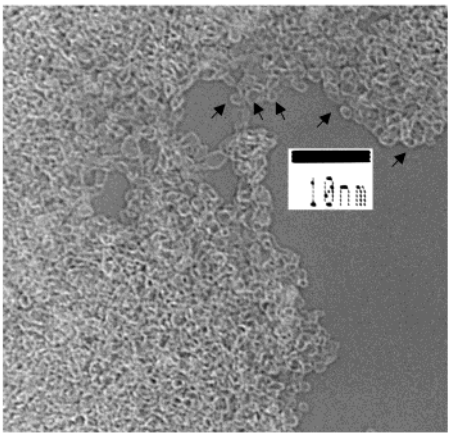

Figure 9. Magnified view of the transmission electron micrograph of extracted sample shown in Figure 8. Arrows at the edges point to near spherical closed shell structures typically in the 1−1.5 nm size range.

no SWNT or graphitic shell particles and was composed completely of nontubular carbonaceous species (compare with the micrograph of the raw sample shown in Figure 1). A selected area from the image shown in Figure 8 is shown at a higher magnification in Figure 9. A vast majority of these nontubular carbonaceous species were found to be distorted spherical or tubular structures with an aspect ratio not more than 3. A few of the closed shell nanostructures are shown by arrows in Figure 9.

As a further test on the chemical identity of the carbonaceous species the fluorinated extracted species were defluorinated by hexylation wih lithium hexyl followed by thermal annealing at 800 °C in an inert ambient. The alkylation procedure was same as that employed in the case of fluorinated, single walled carbon nanotubes.[20,21] Solid-state Raman spectra of the sample is shown in Figure 10 along with the frequencies of the prominent Raman lines. The important outcome from the Raman spectral data is the presence of the low-frequency modes at 230 and 262 cm^{-1}.

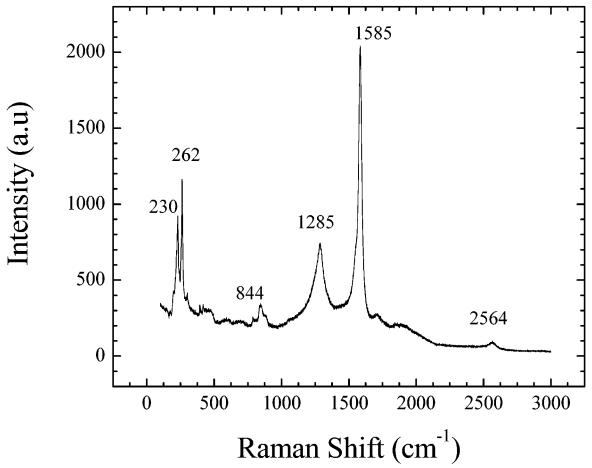

Figure 10. Polarized Raman spectra (λ_{excit} = 780 nm) of the defluorinated extract. Fluorine side groups are removed by alkylating the sample followed by removal of the alkyl groups in a thermal annealing process at 800 °C. The radial modes at 230 and 262 cm^{-1} strongly in favor of a closed shell structure. A strong disorder mode at 1285 cm^{-1}, even after high-temperature thermal annealing suggests possible covalent cross-links between closed shell carbon clusters.

These are the analogous radial modes A_1' and E_2' typical of lower closed shell or curved graphitic sheet structures such as fullerenes.[22,23] The observation of these modes is a clear distinction from other forms of graphitic carbon like highly ordered pyrolytic graphite (HOPG), carbon nanoparticles and glassy carbon which lack these low-frequency radial modes.[24] This serves as additional evidence that the closed shell carbon structures are not formed in-situ during the laser irradiation of nontubular carbon nanoparticles in the LDI mass spectrometer.

Conclusions

A small fraction of high-molecular-weight closed shell carbon clusters are formed along with single-walled carbon nanotubes during the catalytic, high-pressure decomposition of carbon monoxide. Optimal oxidative conditions for the elimination of these fullerenic clusters and carbon-coated iron nanoparticles, with minimal damage to SWNTs have been arrived at. The fullerenic carbon clusters can be desorbed by laser irradiation thus providing for a quantitative estimation by LDI-TOF mass spectrometry with appropriate markers. The carbon clusters could as well be nondestructively removed by chemical methods leaving other forms of carbon intact.

Acknowledgment. The authors thank Robert A. Welch Foundation, Advanced Technology Program of Texas, the National Aeronautics and Space Administration, Office of Naval Research and the National Science Foundation for support of this research.

References and Notes

(1) Endo, M. *CHEMTECH* **1988**, *18*, 568; Tibbetts, G. G.; Bernardo, C. A.; Gorkiewicz, D. W.; Alig, R. L. *Carbon* **1994**, *32*, 569.

(2) Hafner, J. H.; Bronikowski, M. J.; Azamian, B. R.; Nikolaev, P.; Rinzler, A. G.; Colbert, D. T.; Smith, K. A.; Smalley, R. E. *Chem. Phys. Lett*. **1998**, *296*, 195.

(3) Kong, J.; Cassel, A. M.; Dai, H. *Chem. Phys. Lett*. **1998**, *292*, 567.

(4) Nikolaev, P.; Bronikowski, M. J.; Bradley, R. K.; Rohmund, F.; Colbert, D. T.; Smith, K. A.; Smalley, R. E. *Chem. Phys. Lett*. **1999,** *313*, 91.

(5) Bronikowski, M. J.; Willis, P. A.; Colbert, D. T.; Smith, K. A.; Smalley, R. E. *J. Vac. Sci. Technol*. **2001**, *A19*, 1800.

(6) Dillon, A.; Gennet, T.; Jones, K.; Alleman, J.; Parilla, P.; Heben, M. *Adv. Mater*. **1999**, *16*, 1354.

(7) Bandow, S.; Zhao, X.; Ando, Y. *Appl. Phys. A* **1999**, *67*, 23.

(8) Chiang, I. W.; Brinson, B. E.; Smalley, R. E.; Margrave, J. L.; Hauge, R. H. *J. Phys. Chem B* **2001**, *105*, 1157.

(9) Pang, L. S. K.; Saxsby, J. D.; Chatfield, S. P. *J. Phys. Chem*. **1993**, *97*, 6941.

(10) Smalley, R. E.; *Acc. Chem. Res*. **1992**, *25*, 98; Maruyama, Y.; Inabe, T.; Ogata, H.; Achiba, Y.; Suzuki, S.; Kikuchi, K.; Ikemato, I. *Chem. Lett*. **1991**, *10*, 1849.

(11) Diederich, F.; Ettl, R.; Rubun, Y.; Whetten, R. L.; Beck, R.; Alvarez, M.; Anz, S.; Sensharma, D.; Wudl, F.; Khemani, K. C.; Koch, A. *Science* **1991**, *252*, 548.

(12) Gu, Z., et al. To be published.

(13) Heymann, D.; Bachilo, S. M.; Weisman, R. B.; Marriott, T.; Cataldo, F. *Fullerenes Nanotubes Carbohydr. Nanostruct.* **2002**, *10*, 37.

(14) Chiang, I. W.; Brinson, B. E.; Huang, A. Y.; Willis, P. A.; Bronikowski, M. J.; Margrave, J. L.; Smalley, R. E.; Hauge, R. H. *J. Phys. Chem. B* **2001**, *105*, 8297.

(15) O'Brien, S. C.; Heath, J. R.; Curl, R. F.; Smalley, R. E. *J. Chem. Phys*. **1988**, *88*, 220.

(16) Ulmer, G.; Campbell, E. E. B.; Kuhnle, R.; Busmann, H. G.; Hertel, I. V. *Chem. Phys. Lett*. **1991**, *182*, 114.

(17) Liber, C. M.; Chen. C. C. *Solid State Phys* **1994**, *48*, 109.

(18) Cheung, J. T.; Sankur, H.; *CRC Crit. Rev. Solid State Mater. Sci*. **1988,** *15***,** 63.

(19) Chandrabhas, N.; Sood, A. K.; Sundararaman, D.; Raju, S.; Raghunathan, V. S.; Rao, G. V. N.; Sastry, V. S.; Radhakrishnan, T. S. R.; Hariharan, Y.; Bharathi, A.; Sundar, C. S. *Pramana: J. Phys*. **1994**, *42*, 375.

(20) Boul, P. J.; Liu, J.; Mickelson, E. T.; Huffman, C. B.; Ericson, L. M.; Chiang, I. W.; Smith, K. A.; Colbert, D. T.; Hauge, R. H.; Margrave, J. L.; Smalley, R. E. *Chem. Phys. Lett*. **1996**, *260*, 471.

(21) Saini, R. K.; Chiang, I. W.; Peng, H.; Smalley, R. E.; Billups, W. E.; Hauge, R. H.; Margrave, J. L. *J. Am. Chem. Soc*., submitted.

(22) Meilunas, R.; Chang, R. P. H.; Liu, S.; Jensen, M.; Kappes. *J. Appl. Phys*. **1991**, *70*, 5128.

(23) Wang, K. A.; Zhou, P.; Rao, A. M.; Eklund, P. C.; Jishi, R. A.; Dresselhaus, M. S. *Phys. Rev. B* **1993**, *48*, 3501.

(24) Eklund, P. C.; Holden, J. M.; Jishi, R. A. *Carbon* **1995**, *33*, 959.